First-principles study of structural stability, magnetism, and hyperfine coupling in hydrogen clusters adsorbed on graphene

Ahmad Ranjbar,* Mohammad Saeed Bahramy,† Mohammad Khazaei, Hiroshi Mizuseki, and Yoshiyuki Kawazoe
Institute for Materials Research, Tohoku University, Sendai 980-8577, Japan
(Received 31 May 2010; revised manuscript received 1 September 2010; published 26 October 2010)

Using first-principles electronic-structure calculations, we studied the structural and magnetic properties of various hydrogen clusters, including hydrogen monomer, dimers, trimers, tetramers, and hexamers adsorbed on a graphene surface. The magnetic behaviors of such defective systems were shown to strongly depend on the geometrical configuration of hydrogen atoms. The stability of the structures was demonstrated to be dependent on two important factors: the distance between hydrogen atoms and the strength of exchange couplings between the defect-induced magnetic moments. For the magnetic structures, the electron spins populate the quasilocalized p_z-type states on specific carbon atoms. The presence of such quasilocalized p_z-type states was shown to yield relatively strong hyperfine couplings at particular carbon sites in the neighborhood of hydrogen atoms.

DOI: 10.1103/PhysRevB.82.165446 PACS number(s): 75.50.Dd, 81.05.ue, 71.15.Dx

I. INTRODUCTION

Since the discovery of graphene by Novoselov *et al.*,[1] this material has attracted a great deal of attention due to its unique physicochemical properties. Ideal graphene is known to be a nonmagnetic (NM) zero-gap semiconductor, in which the carbon atoms are positioned in a perfect honeycomb lattice. However once doped, the graphene can yield very different electronic properties, depending on the types and/or concentrations of guest species. For instance, very recent experiments by Elias *et al.*[2] indicate that graphene can become a wide-band-gap insulator, known as graphane, if its both sides are alternately covered by hydrogen atoms. On the other hand, the theoretical work by Yang[3] predicts that the similar coverage of both sides of graphene by Li would result in a conductive system. Alternatively, the scanning tunneling microscopy (STM) images by Balog *et al.*[4] further revealed that the chemical modifications caused by hydrogen adsorption on one side of a graphene layer grown on Ir (111) substrate can have substantial impact on its electronic properties. These are a few examples revealing that the electronic-structure properties of graphene can be easily manipulated by chemical adsorption of guest atoms, e.g., hydrogen. It is worth mentioning that with new developments in techniques, such as STM imaging and feedback-controlled lithography, it is now practically feasible to control the desorption of single hydrogen atoms on the surface of materials.[5,6] In this way, one can ideally create predefined patterns of hydrogen clusters on the graphene surfaces. Thus, there seems to be a huge potential for creation of new graphene-based surfaces with highly controlled electronic and magnetic properties in the near future.[4]

As regards magnetism, it is already well understood that hydrogen adsorption may be a promising way to create magnetic graphene surfaces.[7–10] Such magnetism is intriguing, as it does not originate from any magnetic *d*- or *f*-type impurity. While many studies have been carried out to determine the origin of magnetism in single-atom vacancies and hydrogen chemisorption on graphene and graphite surfaces,[11–15] there have been few reports on magnetism induced by clusters of hydrogen atoms.[16–18] This is despite the fact that it has been experimentally found that hydrogen atoms prefer to form different shapes of clusters on carbon-based materials.[19–23] Therefore, detailed studies on stability and magnetic properties of hydrogen clusters on graphene appear to be of essential importance in hydrogen-graphene-based technologies.

Experimentally, the binding energy of hydrogen atoms to a surface is estimated using thermal desorption spectroscopy[23] and the dynamics and coordination of these atoms on the surface can be considered by nuclear-magnetic-resonance experiment.[24–26] The unpaired electron-spin states in such hydrogenated carbon structures can be detected by electron-spin-resonance spectroscopy.[27] Probing hyperfine interactions with magnetic resonance techniques also provides a wealth of information about structure and dynamics of carbon materials.[28] In the present work, based on a set of first-principles electronic-structure calculations, we have accordingly attempted to gain a deeper insight into the structural and magnetic properties of hydrogen clusters adsorbed on the graphene surface. In this regard, we have considered various types of hydrogen clusters, including monomer, dimers, trimers, tetramers, and hexamers. The possible geometries of some of these hydrogen species have already been experimentally or theoretically identified.[19–23,29,30] Below, we compare the relative structural stability of these clusters. We show that, depending on the geometrical arrangement of hydrogen atoms on the surface, the whole system can become magnetic or nonmagnetic. For the magnetic systems, we further calculate and analyze both the Fermi contact and dipolar hyperfine fields for hydrogen atoms and their nearby carbon atoms. The respective hyperfine results are expected to provide valuable information for engineering new electronic devices based on hydrogen-graphene materials.

II. COMPUTATIONAL METHODS

A. Electronic-structure calculations

All the electronic and magnetic calculations were carried out within the context of the density-functional theory (DFT)

using the Perdew-Burke-Ernzerhof (PBE) exchange-correlation functional[31] and the projector augmented wave method,[32] as implemented in the VASP code.[33] We considered a relatively large orthorhombic supercell containing 96 carbon atoms and an appropriate number of (one, two, three, four, and six) hydrogen atoms. To avoid any interaction between the graphene sheet and its periodically repeated images, the lattice constant c of the supercell was considered to be 14 Å. The corresponding Brillouin zone was sampled by a $5\times5\times1$ Monkhorst-Pack mesh. The structures were fully optimized using the conjugated gradient method until the magnitude of force on each ion became less than 0.04 eV/Å. The convergence criterion on the total energy was set to 1×10^{-6} eV. It should be noted that the nonmagnetic states of hydrogenated graphene were obtained through the spin-restricted scheme while the magnetic configurations (ferro and antiferro) were found using spin-polarized calculations.

B. Hyperfine structure calculations

The hyperfine field B_{hf} may be written as a sum of four contributions

$$B_{hf}(I) = B_c + B_{orb} + B_{dip} + B_{lat}, \tag{1}$$

where B_c is the Fermi contact term, and B_{orb} and B_{dip} are the contributions from the on-site magnetic dipolar interaction of the nuclear magnetic moment with the electronic orbital and spin momentum, respectively. B_{latt} is classical dipolar field from all other atoms in the system that carry the magnetic moment. For the magnetic structures in this work, B_c and B_{dip} were the dominant contributions, and were thus the focus of our study. The actual calculation of the hyperfine field follows the approach suggested by Blügel *et al.*[34] The Fermi contact field $\vec{B}_c$ and dipolar hyperfine field $\vec{B}_{dip}$ are computed with

$$\vec{B}_c = \frac{8\pi}{3}\mu_B\vec{m}_{av}, \quad \vec{m}_{av} = \int d\vec{r}'\,\delta_T(\vec{r}')\vec{m}(\vec{r}'), \tag{2}$$

$$\vec{m}(\vec{r}') = \langle\Phi|\vec{\sigma}\delta(\vec{r}-\vec{r}')|\Phi\rangle, \tag{3}$$

$$\delta_T(\vec{r}') = \frac{1}{4\pi r^2}\frac{r_T/2}{[(1+\epsilon/2mc^2)r + r_T/2]^2}, \tag{4}$$

and

$$\vec{B}_{dip} = 2\mu_B\langle\Phi|\frac{S(r)}{r^3}[3(\vec{s}\vec{r})\vec{r}-\vec{s}]|\Phi\rangle, \quad \vec{r} = \vec{r}/r, \tag{5}$$

where $\vec{\sigma}$ and $\vec{s}$ are the Pauli matrices and the electron spin, respectively, μ_B is the Bohr magneton, Φ is the large component of the relativistic wave function, m is the electron mass, $r_T = Ze^2/mc^2$ is the Thomas radius, and $S(\vec{r})$ is the reciprocal of the relativistic mass enhancement that is defined as

$$S(\vec{r}) = \left[1 + \frac{\epsilon - V(\vec{r})}{2mc^2}\right]^{-1} \tag{6}$$

The values of the hyperfine fields in our study were obtained within the DFT framework using full-potential all-electron spin-polarized electronic-structure calculations utilizing the augmented plane-wave plus local-orbital method within the WIEN2K code.[35] For the exchange-correlation potential, we used generalized-gradient approximation in the PBE scheme. Scalar-relativistic effects were included but spin-orbit coupling was neglected. The convergence of the basis set is controlled by a cut-off parameter expressed as the product between the smallest muffin-tin radius in the unit cell (R_{MT}) and the magnitude of the maximum reciprocal-lattice vector (K_{max}). The muffin-tin radii for carbon and hydrogen atoms were selected as 1.32 a.u. and 0.66 a.u., respectively, achieving convergence for a cut-off value of $R_{MT}K_{max}=4.0$. The $1s$ state was selected as a core state while the $2s$ and $2p$ states were treated as valence states. In all the cases, the valence charge densities were expanded up to a G_{max} value of 20.0 a.u.$^{-1}$, equivalent to kinetic energy $E_{cut}=400$ Ry. Finally, the corresponding Brillouin zone was sampled by $5\times5\times1$ k points.

III. RESULTS AND DISCUSSION

A. Stability and magnetic properties

To compare the stability of hydrogen dimer, trimer, tetramer, and hexamer clusters on graphene, we first briefly describe the electronic structure of a single hydrogen atom adsorbed on a graphene sheet, although it has been well studied before.[12,36,37] Throughout this paper, we refer to this system as hydrogen monomer. Experimentally, it has already been proven that a hydrogen atom can be singly adsorbed on graphene or graphite when hydrogen atoms are exposed to the sample at high temperatures.[19,38]

Our calculations show that the adsorption energy, E_A, for a single hydrogen atom adsorbed on graphene is about −0.83 eV. Here, we define the adsorption energy as $E_A = E_{gr+mH} - E_{gr} - mE_H$, where E_{gr+mH}, E_{gr}, and E_H are the total energies obtained for a graphene sheet with m hydrogen atoms adsorbed on it, a perfect graphene sheet and an isolated H atom, respectively. Energetically, the hydrogen atom prefers to be adsorbed on a carbon site rather than on C-C bonds or hollow sites. Considering the fact that the hexagonal primitive cell of the pure graphene has a basis of two carbon atoms, the graphene lattice can be divided into two sublattices A and B, such that all the C atoms in a sublattice are symmetrically transformable to each other by the lattice translation operations (graphene is a *bipartite* lattice). For the sake of simplicity, we suppose that the hydrogen monomer is adsorbed on an A site, labeled as A_0. With respect to A_0, all the other C sites can be labeled as A_n and B_n, where n indicates the nth nearest neighborhood of A_0 (see Fig. 1). The corresponding C-H bond is nearly 1.125 Å, which is slightly longer than the experimentally observed 1.120 Å bond distance for a free CH molecule.[39] As a result of the adsorption, the C atoms below and at the vicinity of H impurity drift outward from the graphene plane so that the bond distances

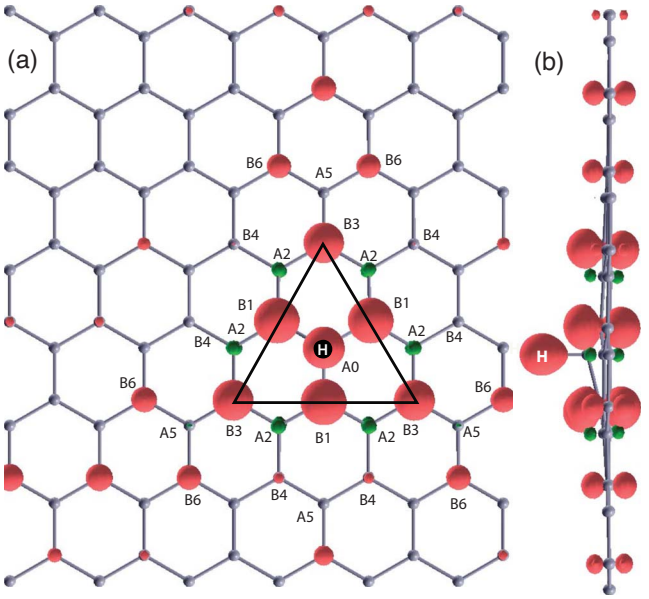

FIG. 1. (Color online) (a) Top view and (b) side view of spin-density distribution around a hydrogen atom adsorbed on the graphene. The red and green (dark and light in the grayscale) isosurfaces correspond to spin-up and spin-down dominated contributions.

between the C atoms at A_0 and B_1 increase to 1.495 Å, whereas the corresponding B_1-A_2 bond lengths decrease to 1.403 Å. Such a trend of increase and decrease in bond lengths appears to be consecutively repeated between the respective A-B and B-A bonds in the neighborhood of A_0. Additionally, the hydrogen atom bounded to its nearest carbon atom makes a hybridized sp^3-like state. This result is consistent with the previous theoretical studies.[12,18]

Furthermore, the adsorption of monomer hydrogen results in spin polarization of the graphene surface with a total magnetic moment of 1 μ_B. Yazyev *et al.* have also concluded that the monomer defect gives rise to strong Stoner ferromagnetism (FM) (Ref. 40) with a magnetic moment of 1 μ_B per defect at all the concentrations they studied.[12] In other words, adsorption of one hydrogen atom at the carbon site in sublattice A introduces a zero-energy state in the complementary sublattice. Such zero-energy states extending over large distances are called quasilocalized states since they show power-law decay.[15,41,42] Our Bader charge analysis[43] reveals that the H atom maintains a small portion of the total magnetic moment while the spin density becomes mainly (about 60% of total magnetic moment) localized on C atoms at B_1 and B_3 sites. The respective local magnetic moments on H and C atoms at B_1, A_2, B_3, B_4, A_5, and B_6 are 0.070, 0.103, 0.00, 0.070, 0.005, 0.00, and 0.021 μ_B. As shown in Fig. 1 and in accordance with the previous calculations,[18,44] the area encompassed by these atoms looks like a triangle, which hereafter we term a spin triangle (ST). Figure 1(b) clearly indicates that the electron spins have populated the quasilocalized p_z-type states on B-type carbon atoms. To better understand the character of these species, the total and orbital-projected density of states (DOS) for the hydrogen monomer system are shown in Fig. 2. For the sake of comparison, the

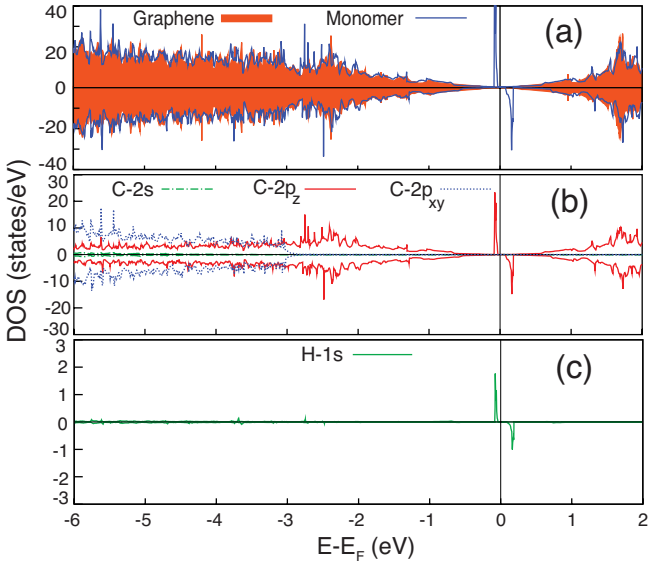

FIG. 2. (Color online) (a) Total density of states as obtained for pure graphene and the monomer, (b) and (c) are the respective partial density of states for carbon and hydrogen atoms in monomer.

figure also contains the corresponding DOS obtained for a pure graphene sheet. The figure clearly shows two sharp peaks close to the Fermi level (E_F) split by exchange interaction; one below E_F in spin-up channel and the other in the opposite spin channel and slightly above E_F. Both peaks are commonly of p_z character and predominantly contributed by C atoms, as discussed earlier, in the B sublattice. This accordingly implies that the spin density is localized in nonbonding π orbitals (due to rather large distance between the nearest B sites). Except for these two peaks, the partial density of states of the monomer system is quite similar to that of pure graphene.

At this point it might be worth mentioning why a nonmagnetic impurity like hydrogen can induce such a delocalized magnetization throughout the graphene, while in a conventional magnetic system, the impurity is usually magnetic and, moreover, maintains a considerable portion of induced

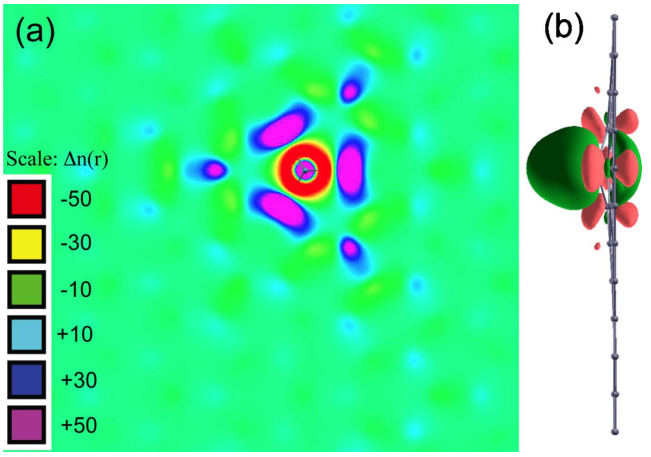

FIG. 3. (Color online) (a) Excess and depletion charge contours. (b) Side view of isosurface for the excess (red) and depletion (green) charge distributions as obtained for monomer.

TABLE I. Total energies (in eV) as obtained for nonmagnetic (E_{NM}), ferromagnetic (E_{FM}), and antiferromagnetic (E_{AFM}) configurations of hydrogen monomer and dimers. E_A and E_a denote the adsorption energies in total and per H atom, respectively. J_x is the dimensionless exchange factor. M_{ST} and M_t refer to the magnetic moment confined inside spin triangle(s) and the total magnetic moment, respectively.

Structures	E_{NM}	E_{FM}	E_{AFM}	E_A	E_a	$E_{FM}-E_{AFM}$	$E_{FM}-E_{NM}$	J_x	M_{ST}	M_t
Monomer	−887.83	−887.88		−0.83	−0.83		−0.05	−0.12	0.59	1.00
D1	−890.96	−890.08		−2.81	−1.41		0.88		0.00	0.00
D3	−890.90	−889.99		−2.75	−1.38		0.91		0.00	0.00
D5	−890.32	−889.70		−2.17	−1.09		0.62		0.00	0.00
D7	−889.92	−889.66		−1.77	−0.89		0.26		0.00	0.00
D2	−889.64	−889.80	−889.69	−1.65	−0.83	−0.11	−0.16	−0.50	1.30	2.00
D4	−889.57	−889.73	−889.65	−1.58	−0.79	−0.08	−0.16	−0.48	1.44	2.00
D6	−889.72	−889.83	−889.76	−1.68	−0.84	−0.07	−0.11	−0.37	1.30	2.00

magnetic moment. The reason can be attributed to the unique two dimensionality of graphene whose distortion requires an imbalance between the C-C bonds, e.g., as described above. Such an imbalance leads to a charge redistribution. As Fig. 3 clearly shows, the redistribution produces excess charges localized on C atoms at B sites. Such excess charges can only be distributed into the nonbonding π orbitals as all the σ orbitals placed in graphene plane are already covalently occupied. As the excess charges in the π orbitals are not sufficient to fully occupy these states, they become partially occupied and hence spin polarized.

Having described the electronic structure of the hydrogen monomer, it is now convenient to extend our discussion to dimer, trimer, tetramer, and hexamer clusters of hydrogen adsorbed on graphene. Prior to any further discussion, we should mention that there are some theoretical studies on stability of particular hydrogen clusters in the literature.[11,18,21,45] In the case of hydrogen dimers, our calculations show that depending on the position of the second H atom with respect to the initial monomer H atom, the entire system can become either magnetic or nonmagnetic. For the former, a total magnetic moment of 2 μ_B is obtained, which is exactly twice as large as that in the monomer system. Assuming that the first hydrogen atom is again adsorbed at the A_0 site, the whole system can exhibit magnetism if the second H atom is adsorbed on one of carbon atoms in the A sublattice, whereas it is totally nonmagnetic if the second H atom is located on any of the host C atoms in the B sublattice. The value of total magnetic moments in a *bipartite* lattice, e.g., graphene can also be obtained by Lieb's theorem.[46] From this theory the total magnetic moment per supercell is $M=|N_B^d-N_A^d|$, where N_A^d and N_B^d are the numbers of defects created in sublattices A and B, respectively. For the nonmagnetic dimers, $N_A^d=N_B^d=1$, consequently, $M=0$. Instead, in the case of magnetic dimers, $N_A^d=2$, $N_B^d=0$, and $M=2$ μ_B. As a result, the total magnetic values of dimers as obtained from DFT calculations are in agreement with Lieb's theorem.

An overall comparison between the nonmagnetic and magnetic dimer structures reveals that the former are energetically more stable than the magnetic ones. Table I lists the total-energy values obtained for different magnetic configurations of dimer species, as well as their respective adsorption energies in total, E_A, and per H atom, E_a. The table clearly indicates that the dimer structures can be categorized in two groups based on their energy values. The first group includes D1, D3, D5, and D7 structures, for which the total energy in nonmagnetic configuration, E_{NM}, is noticeably lower than that in ferromagnetic configuration, E_{FM}. On the other hand, the group consisting of D2, D4, and D6 structures is energetically lower in FM configuration than in NM and antiferromagnetic (AFM) configurations. A more precise comparison reveals that, the highest E_{NM} value in the first group, belonging to D7, still lies below the E_{FM} value of D2, which is the lowest in the second group. This indicates how strongly the stabilization of nonmagnetic dimer species can differ from their magnetic counterparts. It should be noted that in our calculations, we could not obtain E_{AFM} for the nonmagnetic species, while Ferro *et al.*[18] in their recent work apparently could succeed in calculating E_{AFM} for D5 and D7 structures. We believe that the reason for this discrepancy is due to the fact that our calculations allow full structural optimization, whereas Ferro *et al.*[47] only allowed the hydrogen atoms and their surrounding first- and second-nearest neighbors to be relaxed while the rest of the C atoms were fixed at their pure graphene positions.

To explain why the nonmagnetic group of dimers are energetically more stable than the magnetic group, we calculated the adsorption energies for each dimer cluster (see Table I). Evidently, D1, D3, D5, and D7 have relatively lower E_A when compared with the corresponding values for magnetic D2, D4, and D6 structures. Among the first group of clusters, D1 and D3 have the highest stability and, hence, the lowest E_A. This is in accordance with previous experimental and theoretical findings.[18,19] The trend of stability among these species is such that $E_A^{D1}<E_A^{D3}<E_A^{D5}<E_A^{D7}$. On the other hand, a comparison between H-H distances, L_{HH}, reveals that $L_{HH}^{D1}<L_{HH}^{D3}<L_{HH}^{D7}<L_{HH}^{D5}$. Thus, as a general rule it seems that the relative stability of nonmagnetic dimers increases as L_{HH} decreases. The only exception is D5, which is energetically lower than D7 while its L_{HH} is relatively longer than L_{HH}^{D7}. The reason is attributed to the higher monomer spin density at B_6 as compared to that at B_4. This implies that the second hydrogen is expected to make a stronger bonding if it is adsorbed at B_6 than when it is bound to B_4. Considering the fact that the second adsorption sites in D5 and D7 are B_6 and B_4, respectively (see Fig. 4), it is then

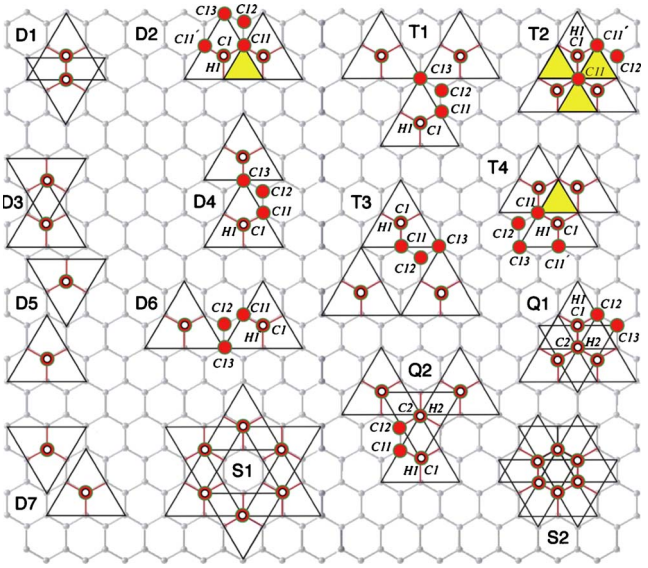

FIG. 4. (Color online) Geometrical configurations of dimers (labeled D1, D2, D3, D4, D5, D6, and D7), trimers (labeled T1, T2, T3, and T4), tetramers (labeled Q1 and Q2), and hexamers (labeled S1 and S2). The yellow (shaded) areas denote the regions commonly shared between the spin triangles. The white points indicate the position of hydrogen atoms. The red filled circles indicate the carbon atoms of interest for hyperfine calculations.

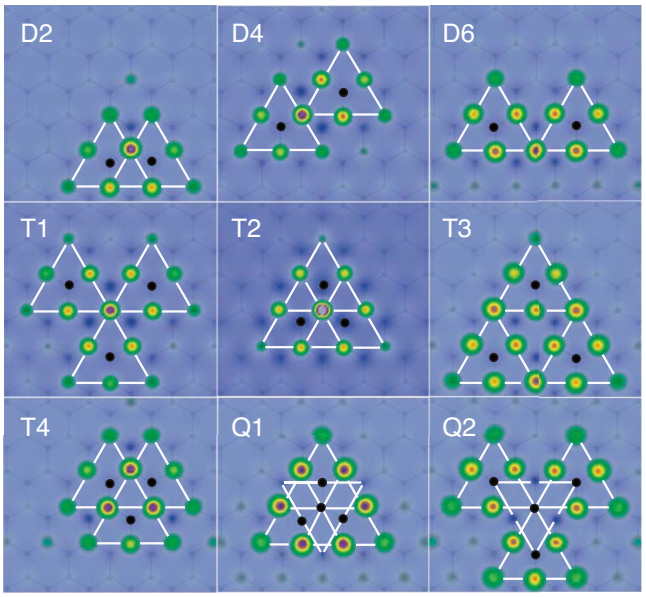

FIG. 5. (Color online) Spin-density distributions of magnetic dimers, trimers, and tetramers mapped on a plane close to the graphene surface. The dark points indicate the position of hydrogen atoms and the spin triangles are shown by white lines.

understandable why D5 is energetically more stable than D7. It should be noted that both host carbon atoms in D1 move out of the graphene plane by 0.78 Å, which is about 0.2 Å larger than the corresponding nonmagnetic dimer values. Additionally, the hydrogen atoms experience lateral displacement[45] by ~0.29 Å relative to the on-top positions (the relaxed L_{HH} of D1 is 2.12 Å instead of 1.56 Å for the strict on-top positions). It is worth mentioning that D1 is the most stable dimer among all others due to this lateral displacement, which is not observed significantly in the other dimer cases.

Recalling our definition of ST in the monomer system, one can clearly see in Fig. 4, that for the nonmagnetic dimers, the two ST's have opposite directions. In other words, the spins of the two triangles are paired. For the sake of simplicity, we suppose that a hydrogen dimer consists of two hydrogen monomers. Moreover, the spin density of a dimer system is assumed to be reproducible by merging the spin densities of the corresponding hydrogen monomers. Accordingly, for the nonmagnetic dimer structures, it turns out that the excess charges are distributed into nonbonding π states at both A and B sites. The short distance between the two neighboring A and B carbon atoms allows the overlap between the partially occupied π states, resulting in the formation of additional π bondings (see the supplementary file[48]). Consequently, the excess charges in nonmagnetic dimers contribute to strengthening the C-C bonds rather than to spin polarization of the graphene surface.

On the other hand, for the D2, D4, and D6 structures where both the hydrogen impurities are adsorbed at A sites, the corresponding ST's appear to be parallel to each other. Consequently, the superposition of monomer spin densities results in an enhancement of the excess charge contributions to the nonbonding π states on carbon atoms at B sties. Owing to the relatively long distance between the B sites, the excess charges would have no overlap with each other and hence no tendency to contribute to any kind of bonding. Thus, the entire system remains magnetic as in the case of a monomer system, *albeit* with a larger magnetic moment ($2\ \mu_B$). The spin density maps corresponding to D2, D4 and D6 are shown in Fig. 5. As the figure clearly shows, the spin-density map of each dimer appears to be made up of the merger of two separate monomer spin maps with each other. Due to the superposition of the monomer spin densities, the commonly shared carbon B sites between the two monomer ST's gain the largest local magnetic moments, as represented in Fig. 5 by dark (brown) and bright (yellow) spots.

To discuss the stability of magnetic dimers, we should consider two important factors. The first factor is the distance between the hydrogen atoms and the second one is the effect of exchange couplings between the defect-induced magnetic moments (electron spins) at B sites. As regards the H-H distance, in contrast to the nonmagnetic dimers, the stability of magnetic dimers increases as the distance between the H atoms increases. This is attributed to the effect of repulsive Coulomb interaction between the electron spins at B sites. Such an interaction evidently is much stronger if the parallel ST's are closer to each other. This further explains why the magnetic dimers are less stable than their nonmagnetic counterparts. In the latter, since the excess charges contribute to the bonding, the electron Coulomb repulsion becomes relatively much lower than that in the former cases, where the excess charges have no option but to partially occupy the nonbonding π states, as described above. According to Table I, the respective total energies of the magnetic dimers can be ordered as $E_{\mathrm{FM}}^{D6} < E_{\mathrm{FM}}^{D2} < E_{\mathrm{FM}}^{D4}$ while a comparison between the H-H distances indicates that $L_{HH}^{D2} < L_{HH}^{D4} < L_{HH}^{D6}$. In other

TABLE II. Total energies (in eV) as obtained for nonmagnetic (E_{NM}) and ferromagnetic (E_{FM}) configurations of hydrogen monomer, trimers, tetramers, and hexamers. E_A and E_a denote the adsorption energies in total and per H atom, respectively. J_x is the dimensionless exchange factor. M_{ST} and M_t refer to the magnetic moment confined inside spin triangle(s) and the total magnetic moment, respectively.

Structures	E_{NM}	E_{FM}	E_A	E_a	$E_{FM}-E_{NM}$	J_x	M_{ST}	M_t
Monomer	−887.83	−887.88	−0.83	−0.83	−0.05	−0.12	0.59	1.00
T1	−891.58	−891.78	−2.53	−0.84	−0.20	−0.77	2.15	3.00
T2	−891.16	−891.76	−2.51	−0.84	−0.60	−1.33	2.22	3.00
T3	−891.60	−891.77	−2.53	−0.84	−0.17	−0.75	2.14	3.00
T4	−891.34	−891.58	−2.33	−0.78	−0.24	−1.20	2.19	3.00
Q1	−895.75	−895.89	−5.54	−1.39	−0.14	−0.33	1.22	2.00
Q2	−895.56	−895.67	−5.32	−1.33	−0.11	−0.25	1.27	2.00
S1	−902.33	−897.29	−9.78	−1.63	5.04		0.00	0.00
S2	−901.97	−897.49	−9.42	−1.57	4.48		0.00	0.00

words, D2 with a smaller L_{HH} is energetically more stable than D4. To rationalize this unexpected trend we should consider another important factor, the exchange interaction between the electron spins at B sites. The importance of this factor was pointed out in Refs. 12 and 18.

Simplifying the Heisenberg model, a dimensionless exchange factor J_x can be defined as

$$J_x \sim -\sum_{i,j} M_i M_j, \tag{7}$$

where M_i and M_j indicate the nearest local magnetic moments at the atomic sites i and j in the same sublattices, respectively. The M_i values were obtained using the Bader method. It should be noted that, for the magnetic hydrogen clusters, the product of the nearest magnetic moments placed in different sublattices is nearly zero. We have accordingly calculated J_x for all magnetic structures. The corresponding results are summarized in Tables I and II. Our calculations show that J_x is minimum for D2 in comparison with the corresponding values obtained for the other dimers. As the exchange coupling between the local magnetic moments acts against the electron Coulomb repulsion, it can thus be seen why D2 energetically lies below D4.

We have considered another group of hydrogen species in our study consisting of three hydrogen atoms adsorbed on the graphene surface in four different configurations, as shown in Fig. 4. We call these systems hydrogen trimers and label them T1, T2, T3, and T4, respectively. For each cluster, the three hydrogen atoms are assumed to be symmetrically adsorbed either at A sites or at B sites. The reason for this assumption is based on recently obtained STM images, which indicate a unique pattern of starlike features.[22] The structure corresponding to such a pattern is thought to be formed from a symmetrical arrangement of three hydrogen atoms adsorbed on a graphene (graphite) surface.[22,29] Several trimer configurations, including T1–T4, have been accordingly proposed as possible structures for this pattern. Common to all these trimers is the threefold rotational symmetry of hydrogen arrangements. Such a symmetry constraint implies that the hydrogen impurities can only be adsorbed at either A or B sites.

Our calculations reveal that hydrogen trimers are all magnetic with a total magnetic moment of 3 μ_B. This is in accordance with our discussion for hydrogen dimers where we showed that if the impurities are in the same sublattice, the whole structure becomes magnetic with a magnetic moment proportional to the number of hydrogen atoms. Lieb's theorem also predicts the same total magnetic value ($N_A^d=3$, $N_B^d=0$, and $M=3$ μ_B). As shown in Table II, the ferromagnetic configurations of the trimers are energetically more stable than the corresponding nonmagnetic configurations by at least (most) 0.17 eV (0.60 eV) for T3 (T2). More importantly, the energy difference between the ferromagnetic and nonmagnetic configurations $E_{FM}-E_{NM}$ of the magnetic dimers and trimers is several times larger than that for the monomer. On the other hand, the calculated E_a values for all the magnetic dimers and trimers are nearly the same as that for the monomer, ~−0.84 eV (see Tables I and II). In other words, while such species yield a stronger tendency toward ferromagnetism than a monomer, there seems to be no noticeable change in the adsorption strength of hydrogen atoms, if they are at either A or B sites.

Similar to what was seen in magnetic dimers, the spin triangles corresponding to T1, T2, T3, and T4 are aligned parallel to each other. Again, the spin-density map of each trimer appears to be reproducible by merging the spin densities of three independent monomers (see Fig. 5). As expected, the local magnetizations are substantially pronounced on carbon B atoms commonly shared between the three ST's. Moreover, the stability of hydrogen trimers can be described in terms of two competitive factors, the H-H distance and the exchange coupling. In other words, the trimers with shorter H-H distances experience stronger electron Coulomb repulsions; however, the exchange couplings between the local spin sites act against the repulsive Coulomb interactions and hence tend to lower the total energy of the system. As an example, the results given in Table II clearly show that T2 with the shortest H-H distances has the largest J_x, ~−1.33. Consequently, its total energy (in magnetic configuration) turns out to be same as the corresponding total-energy values

of structures with much longer L_{HH}, namely, T1 and T3. Interestingly, T2 has also the largest energy difference, $E_{\mathrm{FM}}-E_{\mathrm{NM}}$ (−0.6 eV), in comparison with the other trimers. This is another indication that the exchange coupling in T2 is substantially strong. Such a strong tendency for exchange coupling can be schematically elucidated by comparing the areas commonly shared between ST's of each trimer. These areas are considered to maintain a large portion of spin density and hence, to dominate the exchange couplings. As Fig. 4 depicts, such areas are much larger in T2 in comparison with any other trimer, showing why J_x is so high in this structure. For T4, while its J_x seems to be somewhat large, the Coulomb repulsion is comparatively strong so that T4 is found to be energetically the least stable configuration among the trimers.

Next, we consider the adsorption of hydrogen tetramer clusters on graphene. For the sake of simplicity, we focus our attention only on two tetramer configurations, termed Q1 and Q2. The geometrical arrangement of each structure has been demonstrated in Fig. 4. The former (latter) can be constructed by adding an additional hydrogen atom on top of the central carbon atom of T2 (T1). In both configurations, the central carbon atoms are B type, while as described above, the other three adsorption sites are A type. This implies that the ST corresponding to the central hydrogen atom should be aligned opposite to the other three ST's. Therefore, for both Q1 and Q2, the total magnetic moment is expected to be 2 μ_B. Our calculations confirm such a smaller magnetization in Q1 and Q2. Lieb's theorem also predicts $M=|N_A^d-N_B^d|=|3-1|=2$ μ_B, which is the same as our DFT results. While the addition of a new hydrogen atom to T1 and T2 lowers the magnetization to 2 μ_B, it enhances the stability of the final products. As shown in Table II, the E_a values calculated for Q1 and Q2 are −1.39 eV and −1.33 eV, respectively. These values are much lower than the corresponding values for magnetic dimers and trimers and well comparable with the E_a values obtained for the most stable nonmagnetic dimers, D1 and D3. A detailed Bader analysis indicates that the central carbon B sites at T1 and T2 have local magnetic moments of 0.27 μ_B and 0.78 μ_B, respectively, substantially larger than that at any other carbon sites. The adsorption of hydrogen at these sites results in quenching of the surface magnetism at and in the vicinity of central carbons. In other words, the 1s electron of the additional hydrogen atom is paired with the partially occupied nonbonding π orbital of the central carbon atom, leading to formation of a new sp^3-like C-H bond. Such a covalent bonding subsequently reduces the Coulomb interaction among the unpaired electrons. Furthermore it partly quenches the structural stress induced by the other C-H bonds throughout the graphene surface. As a result, the adsorption of hydrogen atoms in Q1 and Q2 configurations is energetically more favorable than that in magnetic dimer and trimer configurations.

As the final cases, the adsorption of hydrogen hexamer clusters on graphene in two different configurations, S1 and S2, has been also considered. The structure corresponding to each hexamer is illustrated in Fig. 4. As the figure shows, in both configurations, three of the hydrogen atoms are at A sites and the other three are at B sites. Accordingly, the ST's

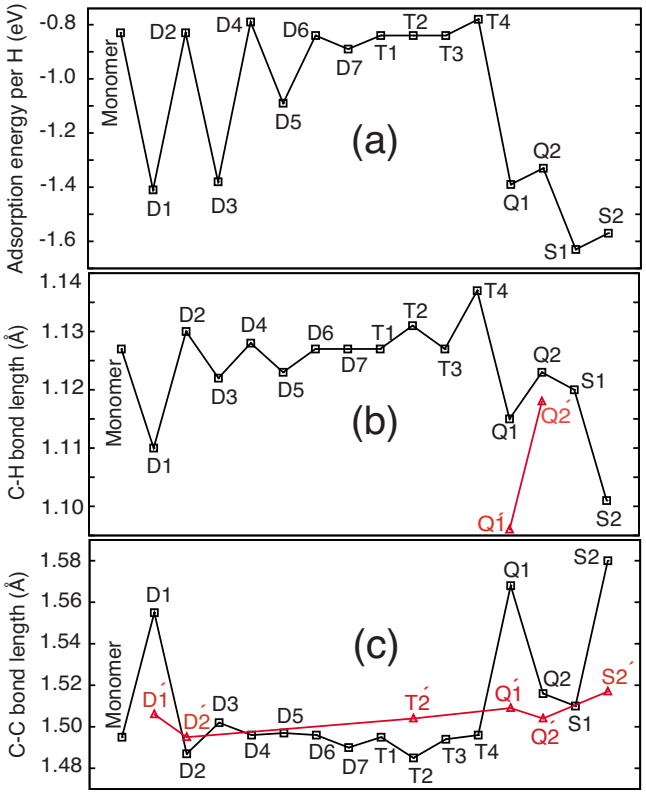

FIG. 6. (Color online) (a) Comparison of (a) E_a (b) C-H bond lengths, and (c) C-C bond lengths as obtained for the monomer, dimers, trimers, tetramers, and hexamers.

of the first three hydrogen atoms become opposite to the other three ST's. As a result, the S1 and S2 structures are nonmagnetic, in agreement with Lieb's theorem. According to Table II, the respective E_a values −1.63 and −1.57 eV obtained for S1 and S2 are the lowest among the other species, and hence these structures are expected to be very stable on graphene. It is worth mentioning that Ferro *et al.*[30] have recently proposed that the S1 hexamer might be the structure responsible for producing the starlike pattern in STM images observed by Hornekær *et al.*[22] The S1 and S2 hexamers are highly symmetrical combinations of the most stable dimers, i.e., D3 and D1, respectively,[30] and their energy differences most probably arise from geometrical constraints, which are weaker in S1 than S2.

To give an overall comparison concerning the stability of all hydrogen clusters considered in this study, the trends of changes in E_a as well as the C-H and C-C bond distances for monomer, dimers, trimers, tetramers, and hexamers are plotted in Fig. 6. As discussed above, the absolute values of E_a for all the magnetic species including the monomer, D2, D4, D6, T1, T2, T3, and T4 are ~0.8 eV, which are considerably smaller than the corresponding values for the other structures. Q1 and Q2 are the only exceptions among the magnetic cases for which $|E_a|$ is as large as those found for the most stable nonmagnetic dimers, D1 and D3. The nonmagnetic hexamers, S1 and S2, as expected, have the largest $|E_a|$ values [see Fig. 6(a)]. The trend of changes in C-H bond lengths reveals that all the magnetic dimers and trimers as well as the monomer have C-H bonds longer than 1.125 Å.

TABLE III. Fermi contact hyperfine filed (B_c) and dipolar hyperfine field (B_{dip}) for the ^{1}H and ^{13}C atoms of interest in the magnetic monomer, dimers, trimers, and tetramers. All hyperfine fields are in kG unit. The labeled hydrogen (H1, H2) and carbon atoms (C1, C2, C11, C11′, C12, and C13) are shown in Fig. 4.

Atoms		Momomer	D2	D4	D6	T1	T2	T3	T4	Q1	Q2
H1(H2)	B_c	15.2	16.6	18.4	15.7	16.1	19.4	16.0	21.0	7.8(−0.2)	9.5(−0.9)
	B_{dip}	0.0	0.0	0.0	0.0	0.0	0.0	0.0	0.0	0.0 (0.0)	0.0 (0.0)
C1(C2)	B_c	−7.2	−10.4	−9.1	−8.1	−9.0	−11.1	−8.9	−13.0	−5.5(0.4)	−5.6(0.9)
	B_{dip}	−0.2	−0.4	−0.3	−0.1	−0.8	−0.7	−0.2	−1.2	1.8(6.2)	0.0(1.71)
C11(C11′)	B_c	7.3	13.4(6.9)	11.7	7.7	10.3	62.0(11.6)	8.9	22.9(8.6)	8.2	6.6
	B_{dip}	−13.1	−17.9(−12.6)	−14.1	−13.3	−14.3	−31.2 (−13.2)	−13.6	−17.3(−12.5)	−12.9	−10.9
C12	B_c	−3.7	−9.6	−10.0	−7.0	−10.1	−6.3	−7.7	−10.1	−5.5	−3.6
	B_{dip}	−9.2	−7.6	−8.4	−8.7	−8.3	−8.2	−8.6	−7.5	−7.9	−7.4
C13	B_c	3.4	5.6	15.1	7.4	12.5		8.2	6.0		
	B_{dip}	−12.8	−13.7	−19.6	−15.6	−19.4		−15.9	−13.3		

In this group, T4 has the longest C-H length, ~1.135 Å [see Fig. 6(a)]. As can be seen in Tables I and II, T4 is interestingly found to have the lowest $|E_a|$ value and the highest total energy among the trimers. On the other hand, the nonmagnetic dimers have relatively shorter C-H bonds. From D1 to D7, the former (latter) has the shortest (longest) C-H length 1.110 Å (1.125 Å). For tetramers, there are two different types of C-H bonds. The first type corresponds to three C-H bonds at *A* sites. The corresponding C-H lengths are comparable with those obtained for nonmagnetic dimers. The second type of C-H bonds is between the fourth hydrogen atom and the central carbon *B* atom. For both Q1 and Q2, the central C-H bond is relatively shorter than the other three ones. The central C-H bond of Q1 is substantially shorter than the C-H bonds of all the other clusters (near 1.095 Å). S1 and S2 are also found to have relatively small C-H bond lengths. In this case, the C-H distances in the latter are significantly shorter than that in the former. Finally, the calculated C-C distances between the hydrogen-bounded carbon atoms and their surrounding neighbors indicate that except for D1, Q1, and S2 with rather large C-C bond lengths, in the other clusters, the C-C bonds are shorter than 1.520 Å [see Fig. 6(c)]. This shows that the hydrogen impurities in D1, Q1, and S2 structures are very strongly attached to the graphene surface so that they can substantially pull out the carbon atoms below them. It is worth mentioning that a significant lateral displacement is also observed in Q1 and S1, as previously discussed for the D1 dimer.

B. Hyperfine couplings

In the magnetic structures, the localization of spin density on H and C atoms implies the presence of hyperfine coupling at their nuclei. Thus, it is worth calculating the Fermi contact field (B_c) and dipolar hyperfine field (B_{dip}) to understand how strongly the spin-polarized wave function of the entire system interacts with the nuclear spins of individual ^{1}H and ^{13}C atoms.

For all the magnetic structures the Fermi contact field (B_c) and dipolar hyperfine field (B_{dip}) were calculated for the hydrogen impurities as well as for the carbon atoms inside the ST's. To avoid any confusion, in Fig. 4, these atoms have been labeled so that they can be easily distinguishable from each other. Table III shows the respective results for the ^{1}H and ^{13}C atoms of interest. Evidently, the B_c values for hydrogen impurities are much smaller than that for a free H atom (~333.4 kG).[49] This is another indication that H pairs its 1*s* electron with host carbon atom and makes a sp^3-like bond. The largest B_c values are obtained for H atoms in T2 and T4. Interestingly, the $|J_x|$ factors corresponding to these structures are also found to be large. On the other hand, Q1 and Q2 with the lowest $|J_x|$ turn out to have the smallest B_c at their H sites. To be precise, hyperfine couplings in the tetramers are negligibly small not only on H atoms but also at the C sites. Therefore, there seems to be a close relationship between the exchange interaction and the hyperfine coupling. The B_c values calculated for the host carbon atoms, C1, are rather small with a negative sign. Considering the fact that the sign of B_c for a free C atom is positive,[50,51] the wave functions at C1-type atoms are expected to be negatively spin polarized. As the dipolar hyperfine fields (B_{dip}) are nearly zero, it is more likely that such a negative spin polarization induces more charge in minority-spin channel of the 2*s* orbitals on these atoms. The rest of carbon sites show a completely different trend of hyperfine coupling. For all these atoms, the B_{dip} contributions are well comparable with B_c values. Since only non-*s*-like states can contribute to B_{dip}, (see the discussions in Ref. 52) such significant B_{dip} contributions imply that the spin density at these carbon sites have *p*-type character. For *B*-type C11 (C11′) and C13 sites, the principal axis for hyperfine anisotropy is in the *z* direction. Accordingly, the spin density is more precisely described to be of p_z character at these sites. This confirms our earlier prediction that the electron spins populate the nonbonding π-type orbitals at carbon *B* sites. While the B_c values corresponding to C11 atoms of all the structures are on the same order as (or slightly different from) the experimental value of the single C atom (~20.5 kG),[50,51] for T2 it surprisingly increases to 62 kG. The respective B_{dip} value (~−31.2 kG) is also the largest value among all B_{dip}'s. The reason is expected to be that the C11 atom, in T2, is commonly shared among the three ST's. As a result, the spin density becomes

strongly localized at this site. Due to the strong exchange coupling of the partially occupied p_z state of C11 with its fully occupied valence 2*s* state, the latter becomes substantially spin polarized so that it makes a huge positive contribution to B_c at C11.

Finally, it should be noted that all the results in this paper, including local magnetic moments and hyperfine couplings, are presented in a constant supercell size and the dependency of the results on defect concentration were not considered. However, it seems that in graphene the nonbonding states induced by hydrogen adsorption are not truly localized but quasilocalized. That is the degree of their localization depends logarithmically on the concentration or equivalently on the supercell size of adsorbed hydrogen atom.[12,41,42,53]

IV. CONCLUSIONS

In conclusion, a series of first-principles density-functional calculations were carried out to study the structural stability of various hydrogen clusters on graphene. Our results showed that depending on the adsorption sites of hydrogen atoms, the system can become magnetic or nonmagnetic. For the nonmagnetic dimers and hexamers as well as the magnetic tetramers, the adsorption energies per H atom were found to be the largest among all the species. The magnetic structures turned out to be structurally less stable than the nonmagnetic systems. The stability of the magnetic configurations was shown to depend on two competitive factors, the distance between hydrogen atoms and the strength of exchange couplings between the defect-induced magnetic moments. While the shorter H-H distance acted to destabilize the whole structure, the exchange coupling tended to lower the total energy and, hence, to enhance the stability of hydrogenated graphene. The hyperfine fields for the magnetic configurations were also calculated. The respective results showed that the commonly shared carbon atoms between the hydrogen spin triangles can exhibit substantially large Fermi contact and dipolar hyperfine fields.

ACKNOWLEDGMENTS

The authors gratefully acknowledge the Center for Computational Materials Science at the Institute for Materials Research for use of its Hitachi SR11000 (Model K2) supercomputer system. M. Khazaei thanks the Japan Society for the Promotion of Science (JSPS) for financial support.

*ranjbar@imr.edu

†Present address: Correlated Electron Research Group, Advanced Science Institute, RIKEN, Hirosawa 2-1, Saitama 351-0198, Japan.

[1] K. S. Novoselov, D. Jiang, F. Schedin, T. J. Booth, V. V. Khotkevich, S. V. Morozov, and A. K. Geim, Proc. Natl. Acad. Sci. U.S.A. **102**, 10451 (2005).

[2] D. C. Elias, R. R. Nair, T. M. G. Mohiuddin, S. V. Morozov, P. Blake, M. P. Halsall, A. C. Ferrari, D. W. Boukhvalov, M. I. Katsnelson, A. K. Geim, and K. S. Novoselov, Science **323**, 610 (2009).

[3] C. Yang, Appl. Phys. Lett. **94**, 163115 (2009).

[4] R. Balog, B. Jørgensen, L. Nilsson, M. Andersen, E. Rienks, M. Bianchi, M. Fanetti, E. Lægsgaard, A. Baraldi, S. Lizzit, Z. Sljivancanin, F. Besenbacher, B. Hammer, T. G. Pedersen, P. Hofmann, and L. Hornekær, Nature Mater. **9**, 315 (2010).

[5] P. Sessi, J. R. Guest, M. Bode, and N. P. Guisinger, Nano Lett. **9**, 4343 (2009).

[6] M. C. Hersam, N. P. Guisinger, and J. W. Lyding, Nanotechnology **11**, 70 (2000).

[7] A. K. Singh and B. I. Yakobson, Nano Lett. **9**, 1540 (2009).

[8] H. Şahin, C. Ataca, and S. Ciraci, Appl. Phys. Lett. **95**, 222510 (2009).

[9] M. Wu, X. Wu, Y. Gao, and X. C. Zeng, J. Phys. Chem. C **114**, 139 (2010).

[10] J. Zhou, Q. Wang, Q. Sun, X. S. Chen, Y. Kawazoe, and P. Jena, Nano Lett. **9**, 3867 (2009).

[11] S. Casolo, O. M. Lovvik, R. Martinazzo, and G. F. Tantardini, J. Chem. Phys. **130**, 054704 (2009).

[12] O. V. Yazyev and L. Helm, Phys. Rev. B **75**, 125408 (2007).

[13] J. J. Palacios, J. Fernández-Rossier, and L. Brey, Phys. Rev. B **77**, 195428 (2008).

[14] O. V. Yazyev, Phys. Rev. Lett. **101**, 037203 (2008).

[15] O. V. Yazyev, Rep. Prog. Phys. **73**, 056501 (2010).

[16] D. W. Boukhvalov, M. I. Katsnelson, and A. I. Lichtenstein, Phys. Rev. B **77**, 035427 (2008).

[17] T. Roman, W. A. Dio, H. Nakanishi, H. Kasai, T. Sugimoto, and K. Tange, Carbon **45**, 218 (2007).

[18] Y. Ferro, D. Teillet-Billy, N. Rougeau, V. Sidis, S. Morisset, and A. Allouche, Phys. Rev. B **78**, 085417 (2008).

[19] R. Balog, B. Jørgensen, J. Wells, E. Lægsgaard, P. Hofmann, F. Besenbacher, and L. Hornekær, J. Am. Chem. Soc. **131**, 8744 (2009).

[20] L. Hornekær, Ž. Šljivančanin, W. Xu, R. Otero, E. Rauls, I. Stensgaard, E. Lægsgaard, B. Hammer, and F. Besenbacher, Phys. Rev. Lett. **96**, 156104 (2006).

[21] L. Hornekær, E. Rauls, W. Xu, Ž. Šljivančanin, R. Otero, I. Stensgaard, E. Lægsgaard, B. Hammer, and F. Besenbacher, Phys. Rev. Lett. **97**, 186102 (2006).

[22] L. Hornekær, W. Xu, R. Otero, E. Lægsgaard, and F. Besenbacher, Chem. Phys. Lett. **446**, 237 (2007).

[23] A. Andree, M. L. Lay, T. Zecho, and J. Küpper, Chem. Phys. Lett. **425**, 99 (2006).

[24] G. Majer, U. Eberle, F. Kimmerle, E. Stanik, and S. Orimo, Physica B **328**, 81 (2003).

[25] E. Stanik, S. Orimo, T. Ichikawa, and H. Fujji, J. Appl. Phys. **98**, 044302 (2005).

[26] G. Majer, E. Stanik, and S. Orimo, J. Alloys Compd. **356**, 617 (2003).

[27] C. I. Smith, H. Miyaoka, T. Ichikawa, M. O. Jones, J. Harmer, W. Ishida, P. P. Edwards, Y. Kojima, and H. Fuji, J. Phys. Chem. C **113**, 5409 (2009).

[28] O. V. Yazyev, Nano Lett. **8**, 1011 (2008).

[29] M. Khazaei, M. S. Bahramy, A. Ranjbar, H. Mizuseki, and Y.

Kawazoe, Carbon **47**, 3306 (2009).
[30] Y. Ferro, S. Morisset, and A. Allouche, Chem. Phys. Lett. **478**, 42 (2009).
[31] J. P. Perdew, K. Burke, and M. Ernzerhof, Phys. Rev. Lett. **77**, 3865 (1996).
[32] P. E. Blöchl, Phys. Rev. B **50**, 17953 (1994).
[33] G. Kresse and J. Furthmüller, Comput. Mater. Sci. **6**, 15 (1996).
[34] S. Blügel, H. Akai, R. Zeller, and P. H. Dederichs, Phys. Rev. B **35**, 3271 (1987).
[35] P. Blaha, K. Schwars, G. K. H. Madsen, D. Kvasnicka, and J. Luitz, *WIEN2K: An Augmented Plane Wave*+Local Orbitals: Program for Calculating Crystal Properties (Vienna University of Technology, Vienna, Austria, 2001).
[36] L. Jeloaica and V. Sidis, Chem. Phys. Lett. **300**, 157 (1999).
[37] X. Sha and B. Jackson, Surf. Sci. **496**, 318 (2002).
[38] T. Zecho, A. Güttler, X. Sha, B. Jackson, J. Küppers, J. Chem. Phys. **117**, 8486 (2002).
[39] D. R. Lide, *Handbook of Chemistry and Physics*, 85th ed. (CRC, Boca Raton, 2004), p. 919.
[40] P. Mohn, *Magnetism in the Solid State* (Springer-Verlag, Berlin, 2003).
[41] V. M. Pereira, F. Guinea, J. M. B. Lopes dos Santos, N. M. R. Peres, and A. H. Castro Neto, Phys. Rev. Lett. **96**, 036801 (2006).
[42] Wen-Min Huang, Jian-Ming Tang, and Hsiu-Hau Lin, Phys. Rev. B **80**, 121404(R) (2009).
[43] R. F. W. Bader, *Atoms in Molecules: A Quantum Theory* (Oxford University Press, New York, 1990).
[44] D. Teillet-Billy, N. Rougeau, V. V. Ivanovskaya, and V. Sidis, Int. J. Quantum Chem. **110**, 2231 (2010).
[45] N. Rougeau, D. Teillet-Billy, and V. Sidis, Chem. Phys. Lett. **431**, 135 (2006).
[46] E. H. Lieb, Phys. Rev. Lett. **62**, 1201 (1989).
[47] In order to confirm the accuracy of our statement, we performed a similar calculation at the same theoretical level as what has been described in the paper of Ferro *et al.* In other words, instead of doing a full structural optimization, we only allowed hydrogen and its first and second neighbors to relax. As expected we obtained the same results as those reported by Ferro *et al.*
[48] See supplementary material at http://link.aps.org/supplemental/10.1103/PhysRevB.82.165446 for side view and top view of the excess (red) and depletion (green) charge isosurfaces for hydrogen clusters adsorbed on a graphene sheet.
[49] W. Weltner, Jr., *Magnetic Atoms and Molecules* (Dover, New York, 1989), and references therein.
[50] J. R. Macdonald and R. M. Golding, Theor. Chim. Acta **47**, 1 (1978).
[51] J. S. M. Harvey, L. Evans, and H. Lew, Can. J. Phys. **50**, 1719 (1972).
[52] M. S. Bahramy, M. H. F. Sluiter, and Y. Kawazoe, Phys. Rev. B **73**, 045111 (2006).
[53] V. M. Pereira, J. M. B. Lopes dos Santos, and A. H. Castro Neto, Phys. Rev. B **77**, 115109 (2008).